Dalton Transactions

ROYAL SOCIETY OF CHEMISTRY

COMMUNICATION

View Article Online
View Journal | View Issue

Cite this: *Dalton Trans.*, 2024, **53**, 12047

Received 21st May 2024,
Accepted 3rd July 2024

DOI: 10.1039/d4dt01488j

rsc.li/dalton

Emissive supramolecular ionic crystals combining a red-NIR phosphorescent $[Re_6Se_8CN_6]^{4-}$ cluster anion and a blue fluorescent tetraphenylethene counter-cation†

Ilya V. Kashnik,[a,b] Marie Cordier,[a] Konstantin A. Brylev,[b] Pierre-Antoine Bouit,*[a] Stéphane Cordier[a] and Yann Molard*[a]

A blue fluorescent tetraphenylethylene-based dication and a red-NIR phosphorescent rhenium octahedral cluster tetra-anion are associated electrostatically to generate a supramolecular ionic framework which crystallizes in the *P*$\bar{1}$ centric space group. The emission properties of the hybrids are studied in the crystalline state and in solution revealing a resonant energy transfer and a high sensitivity toward oxygen.

Introduction

Luminescent hybrid organic–inorganic materials have emerged as a fascinating class of compounds, merging the unique properties of the organic and inorganic components. This flourishing research field holds significant promise for the development of advanced materials with tailored optical properties, spanning across fields including optoelectronics, housing, energy, optics, health, diagnosis, *etc.*[1,2] The versatility of these materials extends beyond classical luminescent systems, encompassing functionalities. They exhibit great promise in sensing applications, where their sensitivity to external stimuli (changes in temperature, pH, and analyte concentration) can be utilized in sensors. In parallel, luminescent frameworks based on emissive cations or Aggregation Induced Emission (AIE)-active luminophores have attracted attention because of their potential applications in optoelectronics, sensing or biology.[3–9] Tetraphenylethenes (TPEs, see one example in Fig. 1) are classical AIE emitters, which proved to be very attractive in the design of Supramolecular/Metal–Organic Frameworks (SOFs/MOFs). They are key components of chemical sensors, bioprobes, and solid-state emissive materials,[6] as they display intense luminescence in the aggregated phase. All these applications are possible as TPEs are straightforwardly synthesized and functionalized.[10] Among the different functionalization approaches, the introduction of cationic heads (ammonium, imidazolium, guanidinium or pyridinium) generates blue emissive ionic materials.[11] However, their association with polyanionic entities to prepare ionic supramolecular frameworks has been neglected.[12] In this work, we chose to combine a blue emitting TPE containing two imidazolium heads, namely $[\mathbf{TPE\text{-}Im_2}]^{2+}$, with a tetra-anionic octahedral rhenium cluster anion showing a red-NIR complementary emission. Our aim herein is to explore potential energy transfers within the hybrid and its ability to generate a white emission.

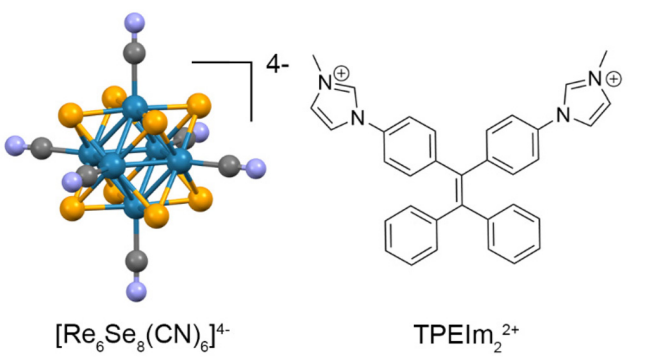

Fig. 1 Representation of the inorganic (colours: blue – rhenium metal atoms, orange – selenium, grey – carbon, and pale blue – nitrogen atoms) (left) and organic (right) polyionic emissive building blocks associated to generate SOFs.

[a]*Université de Rennes, CNRS, ISCR – UMR 6226, ScanMAT – UAR 2025, Rennes F-35000, France. E-mail: yann.molard@univ-rennes.fr, pierre-antoine.bouit@univ-rennes.fr*

[b]*Nikolaev Institute of Inorganic Chemistry SB RAS, 3 Acad. Lavrentiev ave., 630090 Novosibirsk, Russian Federation*

†Electronic supplementary information (ESI) available: Experimental techniques, synthetic procedures, NMR spectra, crystallographic data and structure refinement details, emission decay profiles, and excitation and absorption spectra. CCDC 2355544. For ESI and crystallographic data in CIF or other electronic format see DOI: https://doi.org/10.1039/d4dt01488j

Octahedral rhenium cluster compounds of the general formula $[Re_6Q^i_8L^a_6]^n$ (Q^i = inner ligand; L^a = apical ligand, see Fig. 1) are nanosized inorganic building blocks maintained by metal–metal bonds and obtained *via* a high temperature solid state chemistry route.[13] The metallic Re_6 scaffold is covalently bonded to eight face-capping ligands (μ_3-Q^i) and is stabilized by six apical ones (L^a). They are phosphorescent in the red-NIR region with excited state lifetimes in the microsecond range,[14–16] show a large Stokes shift,[17] and possess excellent photostability.[18]

So far, they have been integrated into nanocomposites without modification of their emission,[19–22] thanks to their primarily metal cluster core centred emission. Furthermore, as their triplet excited state reacts efficiently with O_2,[23] they show great potential as oxygen sensors[24,25] or in photodynamic therapy.[26,27] Surprisingly, although such inorganic emitters have been associated with a large variety of organic monocations, up to now, only a few research groups, including ours, have associated $[Re_6Q_8(CN)_6]^{4-}$ (Q = S or Se) with organic polycations. Combining them with a non-emissive bisamidinium cation leads to a red NIR emissive network in which the stabilization was mainly driven by H-bonds,[28] while using a tetracationic TPE drove the formation of an insoluble red emissive extended network maintained by electrostatic interactions.[29] Usually, emissive materials containing several dyes are able to deliver efficiently a tailored emission that depends on the dye concentration and ratio. However, the degree of interactions between the emitters should also be considered to adjust the emission response toward the applied stimulus. Herein, by lowering the cationic charge on the TPE unit, we expected a higher contribution of the TPE signal to the global emission envelope, compared to previously reported data.[29] Here, we present the first supramolecular ionic framework based on a di-cationic TPE and a tetra-anionic octahedral rhenium cluster complex.

Results and discussion

$[TPE\text{-}Im_2]I_2$ was obtained in a quantitative yield from a dibromo-TPE precursor using C–N coupling followed by methylation (see ESI, Fig. S1†).[30] Mixing **$[TPE\text{-}Im_2]I_2$** at 25 °C with $Cs_4[Re_6Se_8(CN)_6]\cdot 3H_2O$[28] (further denoted as **Cs_4Re**) in methanol or a methanol/water mixture leads to a cationic metathesis and immediate precipitation of **$[TPE\text{-}Im_2]_2[Re_6Se_8(CN)_6]$** (**TPE-Re**) as a powder. This hybrid is only soluble in DMSO which allowed the formation of single crystals suitable for X-ray data collection by slow diffusion of acetone vapor within the solution and its characterization by ^{1}H NMR spectroscopy in DMSO-d_6 (see Fig. S2–S6† for NMR spectra). Surprisingly, compared to **$[TPE\text{-}Im_2]I_2$**, the electrostatic interactions between **$[TPE\text{-}Im_2]^{2+}$** and **$[Re_6Se_8(CN)_6]^{4-}$** do not modify significantly the chemical shift of protons belonging to the imidazolium head: only an upfield shift of $\Delta\delta$ = 0.1 ppm is observed when the iodine counter-anion is replaced by the metal cluster (see Fig. S7†).

According to the single-crystal X-ray diffraction analysis (SCXRD), the crystal structure of **TPE-Re** can be described in triclinic symmetry and the $P\bar{1}$ centric space group. Looking at its representation along the *a* axis (Fig. 2c), it contains an alternation of closely packed organic and inorganic layers. Each cluster unit is in close contact with and sandwiched by eight [**TPE-Im^{2+}**], prohibiting intercluster interactions. Among these eight **$[TPE\text{-}Im_2]^{2+}$** units, six are interacting with the cluster anion *via* one imidazolium ring (Fig. 2b). These interactions occur between protons belonging to the methyl imidazolium moieties with four CN apical ligands (with distances ranging from 2.42 to 2.83 Å) and Se inner ligands (with distances ranging from 2.96 to 3.54 Å). The two remaining apical ligands are in close contacts with protons belonging to a TPE phenyl ring with distances of 2.474 and 2.703 Å. On the other hand, each TPE di-cation is in close contact with four cluster anions (Fig. S8†). Within the organic layer, π–π stacking between non-substituted benzene rings with a shortest C–C distance of 3.541 Å ensures structural cohesion. Along the *b* direction (Fig. 2d), parallel π^+–π^+ stacking interactions between the imidazolium rings in a displaced conformation with distances varying from 4.04 up to 4.90 Å also maintain the organic layer cohesion. This stacking overcomes the repulsive electrostatic interactions and has been previously observed for ionic liquids containing imidazolium rings.[31] Such interactions are also very well visualized in Fig. 2b between the **$[TPE\text{-}Im_2]^{2+}$** moieties localized above and below the inorganic nanocluster. Looking at the **$[TPE\text{-}Im_2]^{2+}$** units, we can observe that the phenyl rings are not perpendicular to the double bond plane. However, photocyclization is unlikely to proceed under UV irradiation, considering the torsion angle values that lie between 47.8° and 63.3°.[32,33] Hence the emission properties of the hybrid were studied by steady state and time dependent emission spectroscopy, in the solid state and in DMSO solution.

Fig. 3 presents the emission spectra recorded from a DMSO solution (aerated and deaerated, black curves) and for a powdered sample (red curve) while the inset shows the drastic colour change of the solution upon deaeration. The photophysical data are presented in Table 1 (see ESI, Fig. S9–S12† for emission decays and analysis). The Förster radius between the two emitters was estimated to be around 3.1 nm (see ESI, Fig. S13† for the overlap between the absorption spectra of the metal cluster and the emission spectrum in the solid state of **$[TPE\text{-}Im_2]^{2+}$**). Therefore, in the solid state, an efficient energy transfer from TPE to the metal cluster is expected considering the distance between the emitters observed by SCXRD. Indeed, looking at the emission spectrum envelope obtained by exciting crystals at 375 nm, such an energy transfer appears to be very efficient: the TPE emission is almost fully quenched and only the red-NIR emission relative to the cluster anion is observed (Fig. 3, red curve). Both starting salts **Cs_4Re** and **$[TPE\text{-}Im_2]I_2$** show similar absolute quantum yield (AQY) values of 6 and 5%, respectively, while the hybrid AQY is also in the same order, around 7%.

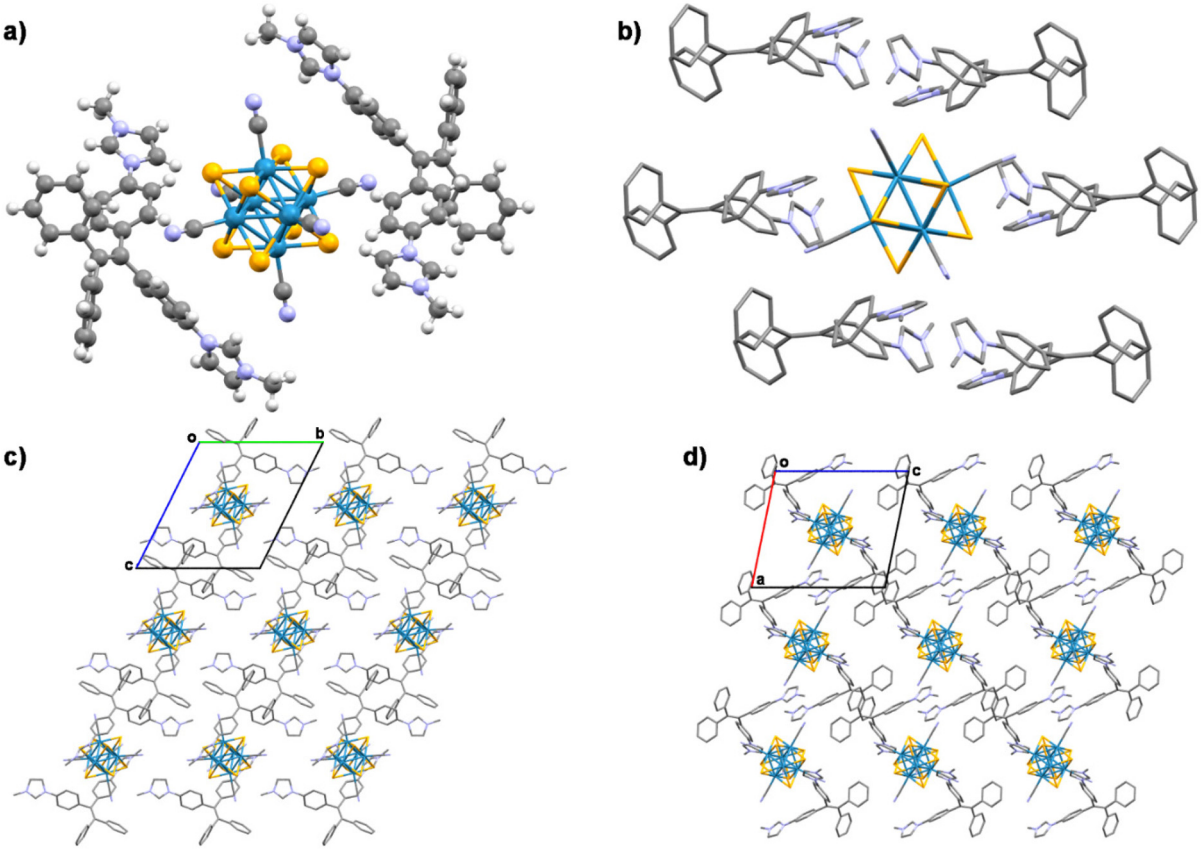

Fig. 2 Representation of **TPE-Re** according to SCXRD (colours: blue – rhenium, orange – selenium, grey – carbon, pale blue – nitrogen, and white – hydrogen atoms); (a) $[Re_6Q_8(CN)_6]^{4-}$ and two $[TPE\text{-}Im_2]^{2+}$ ions; (b) representation of the six **TPE** units for which imidazolium moieties are in close contacts with the **Re** cluster; representation of the crystal structure along the *a* axis (c) and *b* axis (d). In (b), (c) and (d), hydrogen atoms are omitted for clarity.

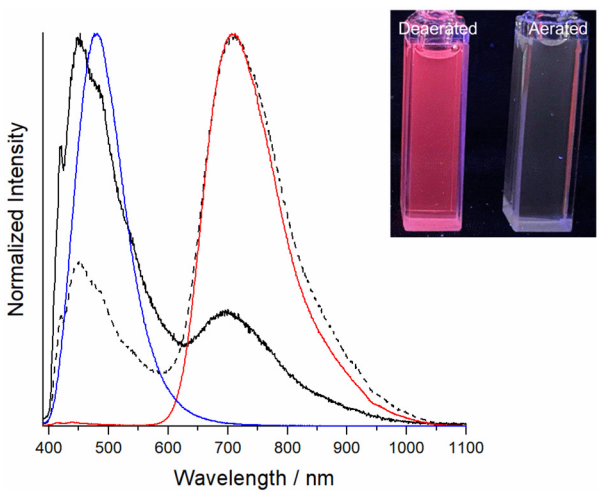

Fig. 3 Emission spectra of $[TPE\text{-}Im_2]I_2$ in the solid state (blue line) and **TPE-Re** in the solid state (red line) and in DMSO solution at 6.5×10^{-5} M (black line; aerated: plain line; deaerated: dashed line; inset: picture of fluorescence cells containing aerated and deaerated DMSO solutions of **TPE-Re**).

In solution, the emission spectrum of **TPE-Re** shows two broad bands with maxima located at 455 and 710 nm, corresponding to the TPE fluorescence and cluster dianion phosphorescence, respectively. The excitation spectra recorded for the two emission maxima are superimposable with an optimal excitation wavelength of 376 nm (see ESI, Fig. S14†).

TPE units are usually poorly emitting in diluted solution because of a combination of phenyl ring rotation, photoisomerization and photocyclization.[32] Therefore, observing the emission of TPE is rather unusual and might be attributed to a conformational restriction due to the interaction of imidazolium heads with the cluster anion, which prohibits all the previously mentioned deactivation processes.

In aerated solution, the cluster emission band is very weak as its emission is essentially quenched by the dissolved O_2. Consequently, the removal of O_2 upon deaeration leads to a large increase of the cluster emission band. Hence, upon deaeration, the solution changes from a pale blue colour to a strong pink one with 1931 CIE coordinates shifting from (x = 0.229, y = 0.249) to (x = 0.296, y = 0.256), as depicted in the inset of Fig. 3.

Table 1 Photophysical data determined in the solid state and in solution at λ_{exc} = 375 nm: emission maxima (λ_{max}), excited state lifetime (τ_i) with the corresponding amplitude (a_i), average lifetime (τ_{av}) and absolute quantum yield (Φ)

Compound	λ_{max}/nm	τ_1 (a_1/%)	τ_2 (a_2/%)	τ_3 (a_3/%)	τ_{av}	Φ /%
[TPE-Im_2]I_2 [a]	480	0.3 ns (48)	0.8 ns (51)	4.9 ns (1)	1.0 ns	6
Cs_4Re[a]	713	1.5 μs (57)	4.0 μs (43)	—	3.2 μs	5
TPE-Re[a]	440	—	—	—	—	7
	710	1.2 μs (71)	5.7 μs (29)	—	4.2 μs	
TPE-Re[b]	455	3.0 ns	—	—	3.0 ns	8
	710	11 μs (92)	17 μs (8)	—	12 μs	

[a] In the solid state. [b] In deaerated DMSO.

Conclusions

A blue emissive TPE derivative bearing two imidazolium heads was synthesized and associated with a red-NIR phosphorescent octahedral rhenium cluster tetra-anion leading to a **[TPE-Im_2]$_2$[$Re_6Se_8(CN)_6$]** hybrid. Such a compound shows poor solubility in DMSO which allowed us to grow single crystals and study their emission properties in the crystalline state and in solution. The luminescence behaviour of the hybrid compound arises from the synergistic interactions between the organic and the inorganic luminophores. While the typical octahedral metal cluster red-NIR emission is observed in the solid state, thanks to the efficient energy transfer from TPE to the metal cluster, the emission colour in solution depends on the presence of dissolved O_2. Hence, the incorporation of an oxygen-sensitive cluster within the hybrid framework should facilitate in the near future the development of responsive materials capable of detecting changes in oxygen concentration with high sensitivity and selectivity which is of major concern in numerous biological and industrial processes, where deviations from optimal oxygen concentrations can have profound implications for functionality and performance. Our progress on the design of such an efficient system based on a metal cluster and TPE will be reported in due course.

Author contributions

I.V.K.: investigation, validation, and writing – review & editing; M.C.: investigation; K.A.B.: supervision, funding acquisition, and writing – review & editing; P.A.B.: conceptualization, supervision, funding acquisition, and writing – review & editing; S.C.: funding acquisition and writing – review & editing; Y.M.: conceptualization, investigation, funding acquisition, supervision, project administration, writing – original draft, and writing – review & editing.

Data availability

The data supporting this article have been included as part of the ESI.† Crystallographic data for **[TPE-Im_2]$_2$[$Re_6Se_8(CN)_6$]** have been deposited at CCDC under CCDC 2355544.†

Conflicts of interest

There are no conflicts to declare.

Acknowledgements

The authors acknowledge ISCR for financial support. The International Associated Laboratory CLUSPOM (2018–2023) and the French Embassy are acknowledged for providing I. V. K. the Vernadski Scholarship for the cotutelle PhD program between France and Russia. I. V. K. and K. A. B. thank the Russian Science Foundation (project 19-73-20196-p).

References

1 C. Sanchez, P. Belleville, M. Popall and L. Nicole, *Chem. Soc. Rev.*, 2011, **40**, 696–753.
2 S. Parola, B. Julián-López, L. D. Carlos and C. Sanchez, *Adv. Funct. Mater.*, 2016, **26**, 6506–6544.
3 M. D. Allendorf, C. A. Bauer, R. K. Bhakta and R. J. T. Houk, *Chem. Soc. Rev.*, 2009, **38**, 1330–1352.
4 J. Rocha, L. D. Carlos, F. A. A. Paz and D. Ananias, *Chem. Soc. Rev.*, 2011, **40**, 926–940.
5 W. P. Lustig, S. Mukherjee, N. D. Rudd, A. V. Desai, J. Li and S. K. Ghosh, *Chem. Soc. Rev.*, 2017, **46**, 3242–3285.
6 J. Mei, N. L. C. Leung, R. T. K. Kwok, J. W. Y. Lam and B. Z. Tang, *Chem. Rev.*, 2015, **115**, 11718–11940.
7 Y. Wen, T. Sheng, X. Zhu, C. Zhuo, S. Su, H. Li, S. Hu, Q.-L. Zhu and X. Wu, *Adv. Mater.*, 2017, **29**, 1700778.
8 Y. Su, J. Yu, Y. Li, S. F. Z. Phua, G. Liu, W. Q. Lim, X. Yang, R. Ganguly, C. Dang, C. Yang and Y. Zhao, *Chem. Commun.*, 2018, **1**, 12.
9 X. He, H. Bi and P. Wei, *J. Mater. Chem. C*, 2023, **11**, 3675–3691.
10 D. D. La, S. V. Bhosale, L. A. Jones and S. V. Bhosale, *ACS Appl. Mater. Interfaces*, 2018, **10**, 12189–12216.
11 J. Knelles, S. Beardsworth, K. Bader, J. R. Bruckner, A. Bühlmeyer, R. Forschner, K. Schweizer, W. Frey, F. Giesselmann, Y. Molard and S. Laschat, *ChemPhysChem*, 2019, **20**, 2210–2216.
12 D. Li, C. Miao, X. Wang, X. Yu, J. Yu and R. Xu, *Chem. Commun.*, 2013, **49**, 9549–9551.

13 F. A. Cotton, *Inorg. Chem.*, 1964, **3**, 1217–1220.
14 S. Cordier, Y. Molard, K. A. Brylev, Y. V. Mironov, F. Grasset, B. Fabre and N. G. Naumov, *J. Cluster Sci.*, 2015, **26**, 53–81.
15 T. G. Gray, C. M. Rudzinski, D. G. Nocera and R. H. Holm, *Inorg. Chem.*, 1999, **38**, 5932–5933.
16 T. G. Gray, C. M. Rudzinski, E. E. Meyer, R. H. Holm and D. G. Nocera, *J. Am. Chem. Soc.*, 2003, **125**, 4755–4770.
17 Y. Zhao and R. R. Lunt, *Adv. Energy Mater.*, 2013, **3**, 1143–1148.
18 M. Amela-Cortes, Y. Molard, S. Paofai, A. Desert, J.-L. Duvail, N. G. Naumov and S. Cordier, *Dalton Trans.*, 2016, **45**, 237–245.
19 M. Robin, W. Kuai, M. Amela-Cortes, S. Cordier, Y. Molard, T. Mohammed-Brahim, E. Jacques and M. Harnois, *ACS Appl. Mater. Interfaces*, 2015, **7**, 21975–21984.
20 Y. Molard, C. Labbe, J. Cardin and S. Cordier, *Adv. Funct. Mater.*, 2013, **23**, 4821–4825.
21 M. Amela-Cortes, A. Garreau, S. Cordier, E. Faulques, J.-L. Duvail and Y. Molard, *J. Mater. Chem. C*, 2014, **2**, 1545–1552.
22 M. Robin, N. Dumait, M. Amela-Cortes, C. Roiland, M. Harnois, E. Jacques, H. Folliot and Y. Molard, *Chem. – Eur. J.*, 2018, **24**, 4825–4829.
23 J. A. Jackson, C. Turro, M. D. Newsham and D. G. Nocera, *J. Phys. Chem.*, 1990, **94**, 4500–4507.
24 R. N. Ghosh, G. L. Baker, C. Ruud and D. G. Nocera, *Appl. Phys. Lett.*, 1999, **75**, 2885–2887.
25 M. Amela-Cortes, S. Paofai, S. Cordier, H. Folliot and Y. Molard, *Chem. Commun.*, 2015, **51**, 8177–8180.
26 K. Kirakci, P. Kubat, M. Dusek, K. Fejfarova, V. Sicha, J. Mosinger and K. Lang, *Eur. J. Inorg. Chem.*, 2012, **19**, 3107–3111.
27 N. Brandhonneur, T. Hatahet, M. Amela-Cortes, Y. Molard, S. Cordier and G. Dollo, *Eur. J. Pharm. Biopharm.*, 2018, **125**, 95–105.
28 A. Ledneva, S. Ferlay, N. G. Naumov, M. Mauro, S. Cordier, N. Kyritsakas and M. W. Hosseini, *New J. Chem.*, 2018, **42**, 11888–11895.
29 I. V. Kashnik, B. Yang, S. S. Yarovoi, T. S. Sukhikh, M. Cordier, G. Taupier, K. A. Brylev, P.-A. Bouit and Y. Molard, *Chem. – Eur. J.*, 2024, **30**, e202400079.
30 X. Zhou, H. Li, Z. Chi, X. Zhang, J. Zhang, B. Xu, Y. Zhang, S. Liu and J. Xu, *New J. Chem.*, 2012, **36**, 685–693.
31 Y.-L. Wang, A. Laaksonen and M. D. Fayer, *J. Phys. Chem. B*, 2017, **121**, 7173–7179.
32 J. Rouillon, C. Monnereau and C. Andraud, *Chem. – Eur. J.*, 2021, **27**, 8003–8007.
33 M. de la Hoz Tomás, M. Yamaguchi, B. Cohen, I. Hisaki and A. Douhal, *Phys. Chem. Chem. Phys.*, 2023, **25**, 18874–18888.